Applied Ocean Research 153 (2024) 104243

Contents lists available at ScienceDirect

Applied Ocean Research

journal homepage: www.elsevier.com/locate/apor

Bayesian modeling and mechanical simulations for fragility curve estimation of the mooring system of marine hydrokinetic devices

Victor Augusto Durães de Faria [a,*], Neda Jamaleddin [b], Anderson Rodrigo de Queiroz [b,c], Mohammed Gabr [b]

[a] Operations Research Department at North Carolina State University, Raleigh, NC, USA
[b] Civil Construction and Environmental Engineering Department at North Carolina State University, Raleigh, NC, USA
[c] Decision Sciences, Economics and Finance Department, School of Business at North Carolina Central University, Durham, NC, USA

ARTICLE INFO

Keywords:
Fragility curves
Mechanical model simulation
Bayesian analysis
Ocean current
Hurricane damage
Risk assessment

ABSTRACT

This work uses Bayesian modeling and mechanical model simulations through the Ansys-AQWA software to construct fragility curve estimates for marine hydrokinetic devices, more specifically, their mooring system. The fragility curves proposed here associate wind speed levels with the risk of damage to the equipment and could be used to better understand the susceptibility of these devices to damage from hurricanes. Our proposed modeling framework uses acoustic Doppler current profiler measurements from a site located off the North Carolina coast and the RM4 conversion device from the Sandia National Laboratory. By evaluating different scenarios with and without dynamic tension in mooring lines due to changes in current velocities caused by extreme wind speeds, our results indicate that the risks of damage may be significant depending not only on the average current velocity but also on the velocity variation.

1. Introduction

With the ever-increasing global climate change and sustainability concerns, the deployment of renewables is expected to increase rapidly in the coming decades. Although this increase is primarily led by solar photovoltaic (PV) installations and onshore wind energy (IEA - International Energy Agency, 2021), substantial investments are also expected in the offshore renewable energy sector. The US government, for example, announced a 30 GW target for offshore wind deployments by 2030 and 110 GW by 2050 (White House, 2021). Additionally, the European Union (EU) has a 300 GW target for offshore wind deployments and a 40 GW target for ocean energy deployments by 2050 (European Commission, 2020a, 2020b).

Despite being in its early development stages, marine hydrokinetic devices are considered to be one of the many promising alternatives to improve the share of renewable energy sources to compose a diversified generation portfolio, potentially reducing energy variability and improving system security. The viability of this technology has been investigated on the Asia east coast (Chang et al., 2015; Liu et al., 2018) and in the states of Florida (Neary et al., 2014; Haas et al., 2013) and North Carolina (Faria et al., 2022) in the United States. Particularly in North Carolina, portfolio optimization and capacity expansion studies have indicated synergies between ocean current and offshore wind as well as ocean current and wave energy technology, leading to reductions in the energy output variability of the equivalent portfolio (Faria et al., 2023).

As the size and frequency of offshore renewable energy deployments increase, a proper understanding of the risks associated with this technology becomes of utmost importance for continuing economic interest in the renewable offshore energy sector. The risks of hurricane damage to many different renewable energy technologies, such as solar PV (Goodman, 2015) and wind turbines (Rose et al., 2013), have been investigated and modeled in the past through the use of fragility curves (Watson and Etemandim, 2020; Faria, 2024), which map the probability of damage to the equipment given certain hurricane speed levels. Similar curves exist for coal power plants, substations, transmission, and distribution lines (Bennett et al., 2021). However, to our knowledge, there is a gap in the literature regarding the definition of fragility curves for ocean current energy systems, indicating an obstacle that inhibits our ability to characterize the susceptibility of these marine hydrokinetic devices to damage from hurricanes.

It is important to mention that although large-scale ocean current

* Corresponding author.
E-mail addresses: vaduraes@ncsu.edu (V.A.D. de Faria), njamale@ncsu.edu (N. Jamaleddin), ardequei@ncsu.edu (A.R. de Queiroz), gabr@ncsu.edu (M. Gabr).

https://doi.org/10.1016/j.apor.2024.104243
Received 7 August 2023; Received in revised form 17 September 2024; Accepted 19 September 2024
Available online 28 September 2024

conversion devices are expected to be submerged about 50 m below the surface (Neary et al., 2014), previous studies have indicated that the influence of extreme weather events can reach such depths. For example, in (Todd et al., 2017) the authors investigated the Gulf Stream conditions during three major hurricanes in 2017, observing transient anomalies for depths of up to 100 m. Similar results were observed by (Ezer, 2018) during Hurricane Matthew in 2016 and by (Oey et al., 2006) during Hurricane Wilma in 2005.

In this work, we postulate that the mooring lines associated with ocean current energy converters pose a critical vulnerability that needs to be considered when constructing fragility curves. Therefore, we propose a novel framework to integrate mechanical model simulations of the mooring system with the statistics obtained from ocean current measurements or hindcasts to produce fragility curve estimates. The ANSYS-AQWA software (ANSYS, 2013) is used to build a mechanical model for the mooring system of a well-known hydrokinetic device, the RM4 developed by the Sandia National Laboratory (Neary et al., 2014), and a Bayesian model is used to estimate the probability distributions of the ocean current variables given extreme wind speed conditions. Finally, this framework is used to construct fragility curves based on ocean current speed measurements from the Gulf Stream in North Carolina. These measurements were obtained using Acoustic Doppler Current Profilers (ADCPs), specialized instruments that measure water velocity using underwater acoustic technology.

The main contributions of this paper can be summarized as follows:

(i) A Bayesian formulation is proposed to perform extreme value analysis for ocean current variables.
(ii) Ansys-AQWA software is used to perform mooring system simulation designs for the RM4 current turbine, considering steady-state and dynamic conditions.
(iii) A framework to connect ocean statistics with mooring system designs is developed to determine fragility curves for hydrokinetic devices, associating extreme weather events (e.g., hurricanes) with the probability of equipment damage.
(iv) A case study using ADCP measurements from the NC coast is performed, providing insights into the ocean conditions in the region and its effect on mooring system modeling.

Our work contributes to a better characterization and definition of the mooring system of ocean current conversion devices, and its results provide an initial assessment of the risks of damage given hurricane-induced conditions. The remainder of this paper is divided as follows: Section 2 presents the models considered in this work, Section 3 presents the case study, detailing the data used and the region investigated, Section 4 shows the simulation results, and Section 5 concludes the paper.

2. Methods

The development of the approach proposed here can be segmented into four steps: (1) Data Acquisition and Treatment; (2) Statistical Analysis to explore the influence of extreme weather events in ocean

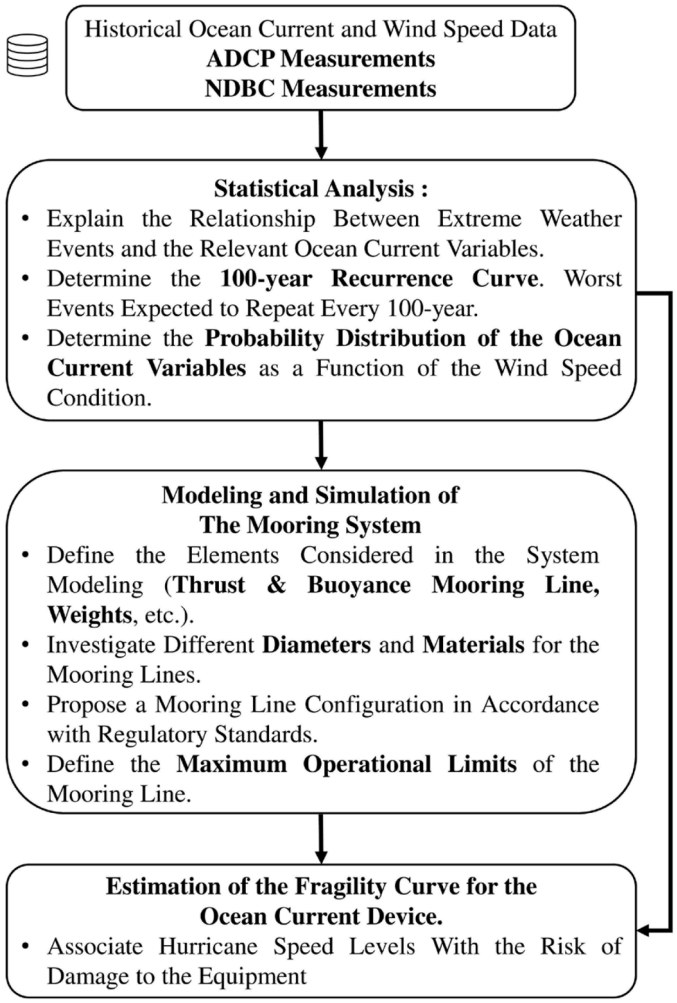

Fig. 1. Models & methods flow diagram.

current variables; (3) Modeling and Simulation of the Mooring System; and (4) Estimation of the Fragility Curve for Ocean Current Devices. Fig. 1 shows a flow diagram with detailed information about these four steps and how they connect in this work.

First, ADCP measurements are used in statistical analysis to determine the set of extreme current events expected to repeat every 100 years (100-year recurrence curve). This data is essential in the definition of the loads induced in the mooring system of the ocean current device. Additionally, wind speed measurements from the National Data Buoy Center (NDBC) are integrated with the ADCP ocean current speed data to determine the probability distribution of the ocean current variables under different wind speed conditions during extreme weather events.

Next, the 100-year recurrent curve from the statistical analysis is used in the modeling of the mooring system of the ocean current device. During this stage, the components of the mooring system are defined and incorporated in the Ansys-AQWA software, such that different line configurations (e.g., materials, diameters) can be investigated until a design configuration capable of enduring the loading associated with the 100-year recurrence curve is specified. Finally, with a suitable mooring system design, the maximum operating limits of the system (above the 100-year curve) are determined.

Lastly, with the maximum operating limits of the mooring system and the probability distribution of the ocean current variables as a function of the wind speed, the fragility curve of the mooring system of the ocean current turbine can be determined, thereby associating the risk of damage to the equipment with different hurricane speed levels.

The following sections provide detailed explanations of each model's structure, parameter selection, and applicability to this specific problem.

2.1. Bayesian modeling

As will be detailed in Sections 2.2 and 2.3, the statistical models developed in this work to compute 100-year ocean current states and the joint probability distribution of extreme wind speeds and ocean current variables are based on Bayesian methodologies. Bayesian models were chosen due to their several advantages, such as their capacity to provide comprehensive uncertainty quantification through posterior distributions and their ability to handle complex dependencies between multiple variables.

Bayesian analysis begins by specifying a prior distribution for each model parameter ($\pi(\boldsymbol{\theta})$), which represents our beliefs about the parameter values before new observations are considered ($\boldsymbol{Y}$). These priors can be uninformative, indicating little prior knowledge, or informative, incorporating existing knowledge or expert judgment (Reich and Ghosh, 2019). While this work utilizes uninformative priors in the models presented in Sections 2.2 and 2.3 for simplicity, the use of informative priors can significantly enhance parameter estimation, especially in contexts where observations are sparse or subject to high variability, as often encountered in extreme value analysis.

After defining prior distributions, likelihood functions are defined ($f(\boldsymbol{Y}|\boldsymbol{\theta})$), which represents the probability of observing the data (Y) given a specific set of parameter values. With these two sets of distributions, Bayes' theorem (1) can be applied to compute the model posterior distribution $P(\boldsymbol{\theta}|Y)$, which provides a full probabilistic description of the model parameters (Reich and Ghosh, 2019). Unlike point estimates produced by Maximum Likelihood Estimation (MLE) models, Bayesian models yield a posterior distribution that captures the range of plausible parameter values along with their associated uncertainties.

$$P(\boldsymbol{\theta}|Y) = \frac{f(\boldsymbol{Y}|\boldsymbol{\theta})\pi(\boldsymbol{\theta})}{\int P(\boldsymbol{Y}|\boldsymbol{\theta})\pi(\boldsymbol{\theta})d\boldsymbol{\theta}} \propto f(\boldsymbol{Y}|\boldsymbol{\theta})\pi(\boldsymbol{\theta}) \tag{1}$$

For most complex models, solving Eq. (1) analytically is highly challenging and often infeasible. In such cases, Markov Chain Monte Carlo (MCMC) methods are employed to estimate the posterior distribution by generating a series of random samples (Reich and Ghosh, 2019). This approach allows for an approximation of the posterior distribution when direct computation is not possible and is the procedure adopted in this work.

2.2. 100-year recurrence curve- bivariate extreme value analysis

Frequently, mooring systems are designed based on extreme conditions that can occur recurrently every 100 years (DNV, 2015; IEC, 2015). Particularly for marine hydrokinetic devices, preliminary mechanical model simulations indicated that the ocean current velocity (S_t) and velocity amplitude variations ($\Delta S_t = S_{t+1} - S_t$) are significant in defining these extreme conditions, as will be shown in Section 4.3.

In general, recurrence curves are constructed by fitting a probability distribution to a set of observations and finding through this distribution the set of extreme events that are expected to repeat only every a certain period of time (e.g., 100 years) (Young et al., 2020; Alves and Young, 2003). The curve that separates this set of extreme 100-year events from the remaining data is defined as the 100-year recurrence curve.

To induce independence between observations in the data set used in the probability distribution construction, not allowing for multiple observations from the same storm, only the peak measurements above a threshold rule are considered, and a minimum distance of 48 h between extreme events is enforced, similar to Young et al. (2020), Caires and Sterl (2004). An extreme event is considered to begin when the threshold is violated upwards and to end when it is violated downwards. However, if amid two events, the time distance between a downward threshold violation and an upward violation is smaller than 48 h, the corresponding observation is considered as a single extreme event.

The threshold rule adopted for the models in this section is defined for both the ocean current velocity (S_t) and velocity variation (ΔS_t). Any measurement pair (S_t, ΔS_t) such that $S_t + \Delta S_t$ is above the 90th percentile is considered to be above the threshold. Furthermore, the peak measurements are also defined through the summation of S_t and ΔS_t.

After defining the set of extreme conditions, two Bayesian models are formulated to explain the existing data. Model I estimates the joint probability distribution of S and ΔS (a single extreme event), and Model II estimates the probability distribution of the number of extreme events in a given time interval.

Model I assumes the ocean current velocity and velocity variations follow a multivariate normal distribution (Eq. (2)), where the mean ocean current speed (μ_s) and speed variation ($\mu_{\Delta s}$) depends on the measurement depth (D), and the variance-covariance matrix ($\boldsymbol{\Sigma}$) is represented through Eqs. (5)–(8), which ensure that $\boldsymbol{\Sigma}$ is positive semi-definite and uninformative (Huang and Wand, 2013). Furthermore, in Eqs. (2)–(9), ρ is the correlation between S and ΔS, a is a constant set to 0.01 to enforce uninformative priors (Reich and Ghosh, 2019), and β are parameters of the model, where $\beta_{1,s}$ associates the mean ocean current speed with the measurement depth and $\beta_{1,\Delta s}$ associates the speed variation with the depth.

Model I: Joint Probability Distribution $(S, \boldsymbol{\Delta S})$

$$(S, \Delta S) \sim Normal(\boldsymbol{\mu}, \boldsymbol{\Sigma}) \tag{2}$$

$$\mu_s = \beta_{0,s} + \beta_{1,s} D \tag{3}$$

$$\mu_{\Delta s} = \beta_{0,\Delta s} + \beta_{1,\Delta s} D \tag{4}$$

$$\sqrt{\Sigma_{11}} \sim Gamma(a, a) \tag{5}$$

$$\sqrt{\Sigma_{22}} \sim Gamma(a, a) \tag{6}$$

$$\Sigma_{12} = \sqrt{\Sigma_{11}\Sigma_{22}} \times \rho \tag{7}$$

$$\rho \sim Uniform(-1, 1) \tag{8}$$

Algorithm 1
100-year recurrence curve estimation.

Inputs: Probability Distributions from Models I and II
Output: 100-year Recurrence Curve
for $i = 1, \ldots, N$:
1) Sample from $Poisson(\lambda \Delta T)$ (10), to determine the number of extreme events that happen in one year ($\Delta T = 365.25\ [days]$). Call Y_i the sampled value.
if $Y_i \neq 0$:
2) Sample from $Normal(\boldsymbol{\mu}, \boldsymbol{\Sigma})$, Y_i times, and name the sampled pairs as $\left(S_{i,j}, \Delta S_{i,j}\right)$, with $j \in \{1, \ldots, Y_i\}$.
3) For the set of values sampled in the previous stage i find the most severe condition among the j indexes. At this step, the most extreme condition (C_i) is defined through the sum of S and ΔS.

$$C_i = \max_j (S_{i,j} + \Delta S_{i,j})$$

Save the S and ΔS values correspondent to C_i as $(S_i, \Delta S_i)$.
end
if $Y_i = 0$: (No extreme scenario)
4) Set $(S_i, \Delta S_i) = (0,0)$, and $C_i = 0$. For iteration purposes, we assign a non-extreme condition as a scenario.
end
end
5) Find the extreme condition c^* ($c^* > 0$) such that

$$\frac{1}{N} \sum 1_{C_i > c^*} \cong 1/100$$

This equation counts the number of events that exceed the severity of c^* and take the average from the total number of events (N). c^* must be chosen such that only one every 100 events/years (each year has only one C_i) exceed c^*.

6) Go back to the samples $(S_i, \Delta S_i)$, and find the curve $F_{100Y}(S, \Delta S)$ that separates the set $\{C_i | C_i > c^*\}$ from the set $\{C_i | C_i < c^*\}$. $F_{100Y}(S, \Delta S)$ is the 100-year recurrence curve.

$$\beta \sim Normal(0, 1/a) \tag{9}$$

Model II assumes that the number of extreme events (Y) occurring in a given time interval (ΔT) follows a Poisson distribution as in (10–12), where λ is the expected number of events per unit of time. This is a well-known class of Bayesian models (Reich and Ghosh, 2019), and the conditional probability distribution of λ given the data is shown in (11). As in Eqs. (2)–(9), a is set equal to 0.01.

Model II: Probability Distribution of the Number of Extreme Events

$$Y \sim Poisson(\lambda \Delta T) \tag{10}$$

$$\lambda \sim Gamma(a, a) \tag{11}$$

$$\lambda | Y \sim Gamma(a + Y, a + \Delta T) \tag{12}$$

Finally, Models I and II are integrated as in Algorithm 1 to determine the 100-year recurrence curve. In this algorithm, we chose N to be the number of iterations necessary for the convergency of the Markov Chain Monte Carlo (MCMC) run (Reich and Ghosh, 2019) of Model I.

The procedure mentioned above is a generalization of the single variable 100-year extreme value analysis (Young et al., 2020; Alves and Young, 2003). With the data presented in Section 3 and the models described in this section, Fig. 6 in Chapter 4 (Results) illustrates the 100-year recurrence curve computed in this work.

2.3. Bayesian statistical modeling of hazardous wind speed conditions

In this section, we propose a model for the joint probability distribution of the ocean current velocity and velocity variation, given extreme wind speed conditions. Model III is mathematically similar to Model I, with the only difference being the mean ocean current speed (μ_s) and speed variation ($\mu_{\Delta s}$) are assumed to depend not only on the measurement depth (D) but also on the measured wind speed (WS) close to the water surface.

Model III: Joint Probability Distribution $(S, \Delta S)$ Under Extreme Winds

$$(S, \Delta S) \sim Normal(\boldsymbol{\mu}, \boldsymbol{\Sigma}) \tag{13}$$

$$\mu_s = \beta_{0,s} + \beta_{1,s} D + \beta_{2,s} WS \tag{14}$$

$$\mu_{\Delta s} = \beta_{0,\Delta s} + \beta_{1,\Delta s} D + \beta_{2,\Delta s} WS \tag{15}$$

With β and $\boldsymbol{\Sigma}$ and priors following Equations $(5-9)$ (16)

For this model, since the interest is in evaluating the impact of extreme wind on ocean current variables, the extreme events are defined based on the threshold rule (Young et al., 2020; Alves and Young, 2003) using the 90th percentile of the wind speed measurements and not on $S_t + \Delta S_t$ as in Models I and II.

For each extreme event mapped in the dataset, the maximum wind speed (WS_{t_1}) and the $(S_{t_2}, \Delta S_{t_2})$ pair correspondent to the maximum $S_{t_2} + \Delta S_{t_2}$ measurement is assigned to Model III. Notice that in this data processing, the time (t_1) of the critical wind speed condition may be different from the time (t_2) of the critical ocean current condition.

Due to limitations in data availability for high-resolution ocean current speed data, as will be discussed in Section 3, a linear correlation model was chosen for analyzing the effects between extreme ocean currents and wind speed conditions. Nonetheless, with advancements in data collection and availability, future research should also investigate possible non-linear effects and identify those with statistical significance.

2.4. Mooring system modeling

The deployment of offshore floating marine hydrokinetic devices

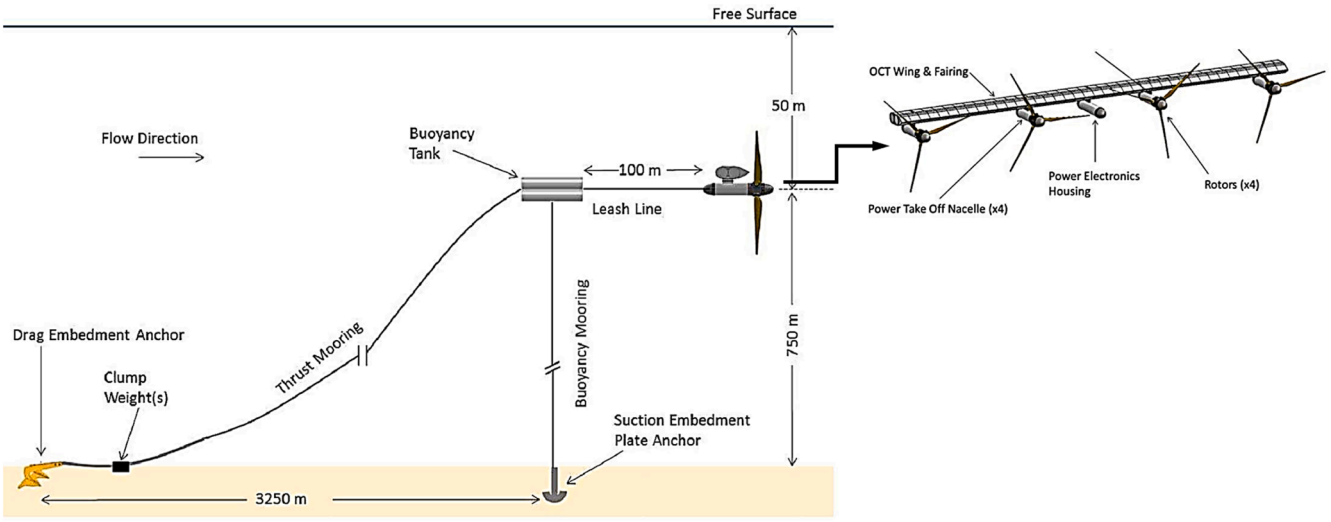

Fig. 2. RM4 device configuration and dimensions (Neary et al., 2014).

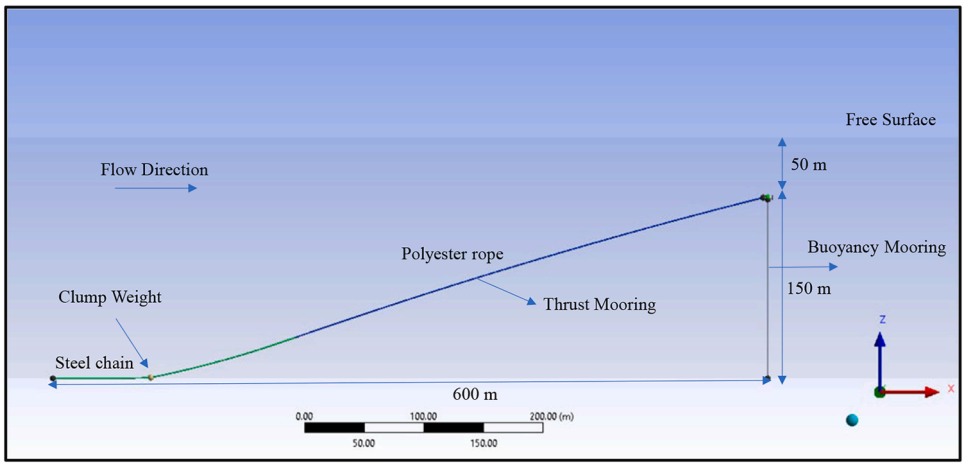

Fig. 3. Schematic model in ANSYS-AQWA.

requires the installation of mooring systems. By providing restoring force, the mooring system keeps the marine hydrokinetic device stationary, within tolerance, as environmental forces cause it to be displaced from its equilibrium position (Xu et al., 2021). Catenary and taut moorings are among the most common mooring configurations available for use by the marine hydrokinetic industry. Catenary mooring derives its compliance from the change in suspended line weight. In the case of taut mooring, compliance is mainly from the elastic stretch of the lines and is related to the stiffness/modulus of the material from which the mooring line is made (DNV, 2010).

As the focus of this work is on evaluating the mooring of ocean current devices, the RM4 from Sandia (Neary et al., 2014) was used as a basis for the system parametrization. The RM4 has four rotors, each with a 1 MW power rating, yielding a total of 4 MW. The device uses a buoyancy tank within the wing and five nacelles to keep its position within the water column.

Fig. 2 shows a diagram of the device (Neary et al., 2014); as can be seen, the mooring system consists of buoyancy and thrust mooring lines secured to the seafloor. The thrust mooring line accommodates the tension from the thrust load produced by the four turbines under various operational conditions, and the buoyancy mooring(s) accommodates the tension from the buoyancy tank needed to keep the device at an approximately stationary position within the water column. The clump weight attached to the thrust mooring line at the seabed serves to render the forces acting on the drag embedment anchor to be mainly oriented horizontally, as drag anchors have minimal vertical pullout capacity (VanZwieten et al., 2014).

For subsea profile, a condition representative of a potential deployment site in North Carolina is considered with a water depth of 200 m and the RM4 submerged at 50 m deep (Fig. 3).

Fig. 3 shows the simulated model in ANSYS-AQWA. For the sake of simplicity, only the buoyancy tank, the mooring lines, and the clump weight have been modeled. A 4:1 mooring scope is considered, allowing the mooring system to accommodate the necessary thrust load from the device without requiring large buoyancy (Neary et al., 2014), and the buoyancy tank is sized to provide sufficient up-force to keep the taut mooring line in tension.

The buoyancy tank is modeled as a hollow steel cylinder with a diameter of 6 m, a wall thickness of 64 mm, and a length of 16 m, at a depth of 50 m. These geometrical values provide a buoyancy tank dry mass of 150 mt and a net buoyancy force of 3020 kN after accounting for the tank's weight. Additionally, it has a Gyration radius of 2.83 m about the x-direction and 5 m about the y and z directions.

According to the RM4 specifications (Neary et al., 2014), an extreme hydrodynamic loading condition based on a 2.4 m/s current velocity will produce a 1400 kN thrust load on a rotor. This thrust force is modeled by applying a force vector of the same value on the buoyancy tank towards the x-direction. The thrust force (T_h) on each rotor of the

simulated ocean current turbine at different current velocities is estimated by Eq. (17), where ρ_w is the water density, A_R is the rotor blades' swept area, C_T is the thrust coefficient, and U is the current velocity (VanZwieten et al., 2014). Water density is equal to 1025 kg/m^3, rotor diameter is 33 m per the reference model, and C_T is assumed to be 0.55. Considering U equal to 2.4 m/s would yield a thrust load of 1400 kN (Neary et al., 2014). The thrust force is determined for various current velocities using Eq. (17).

$$T_h = 0.5\rho_w C_T A_R U^2 = 0.125\pi\rho_w C_T D^2 U^2 \quad (17)$$

The water current force (F_{cs}) acting on a cylinder can be estimated using the following formula (Kuang et al., 2022):

$$F_{cs} = 0.5\, C_d A \rho_w U^2 \quad (18)$$

Where C_d is the drag coefficient of the water flow, which is assumed 1.0 for a cylinder parallel to the flow. A is the projected area of the buoyancy tank in the direction perpendicular to the incident water current.

A coupled dynamic analysis is used to determine the maximum tension in the mooring system. In this approach, the complete system of equations accounting for the rigid body of the device and the slender body model for the mooring lines are solved simultaneously using a non-linear time domain approach (DNV, 2010). The dynamic analysis considers the impact of added mass, dampening, fluid acceleration, and the relative velocity between the mooring system and fluid (Rahayuningsih et al., 2020).

The design is established according to the Det Norske Veritas (DNV) Offshore Requirements for Position Moorings (DNV, 2015) since there are no offshore standards that are specific for ocean current turbines. For ultimate limit State (ULS) criterion, it is recommended to use partial safety factors in the case of dynamic analysis. The simulated moored turbine system is characterized as a Class 1 Consequence Class, in which possible consequences of a mooring system failure include loss of human life and significant economic damages. Accordingly, a partial safety factor (γ_{dyn}) of 1.5 for dynamic tension and a partial safety factor (γ_{mean}) equal to 1.1 for mean equilibrium tension are specified. In this case, acceptable mooring component strength is achieved when (19) is satisfied (DNV, 2015). In this inequality, CBS is the catalog break strength of the mooring line, which is multiplied by 0.95 as recommended in DNV (2015), T_{mean} is the equilibrium tension and T_{dyn} is the dynamic tension.

$$T_{mean}\gamma_{mean} + T_{dyn}\gamma_{dyn} \leq 0.95CBS \quad (19)$$

2.5. Fragility curve estimate for ocean current devices

Fragility curves relate a specific physical condition with the probability of damage to the equipment/structure. In this work, for a given hurricane speed level (WS) and turbine depth (D), different ocean current speeds (S) and speed variations (ΔS) may occur. These conditions are statistically represented by the Bayesian Model III, and from this model, the conditional probability distribution of the ocean current variables $(S, \Delta S \mid WS,\ D)$ can be obtained.

In this context, if the mooring system's operation limits are defined (e.g., maximum admissible S and ΔS curve), the probability of damage to mooring lines and the equipment can be computed as in (20). In other words, the fragility curves can be determined by varying the wind speed levels and computing the probability of the system exceeding its operational limits. This work determined this probability by computing the ratio of samples from the Bayesian model that fall outside the device's limits of operation at a given wind speed. This computation considered all possible distribution parameters estimated by the Bayesian model and their respective probabilities.

Uncertainty in the process of computing a device fragility curve stems from both the device's structural capacity and the statistical modeling of extreme events. Different operational limits are often investigated to help understand how the probability of damage to the device is affected, as will be demonstrated in Section 4. However, recent research by Ceferino et al. (2023), Kakareko et al. (2021) highlights the use of Bayesian frameworks to account for uncertainties in extreme event statistics. These studies use the Bayesian model to provide different parameters for the extreme value distribution and compute fragility curves for each individual parametrization, thereby providing insights into the uncertainty of the estimated fragility curves. Although this approach is not utilized in this work, it is recommended as a potential direction for future research.

$$1 - P((S, \Delta S) \in \textit{Limit of Operation} \mid WS,\ D)) \quad (20)$$

3. Case study

As a case study, we focus on a portion of the US east coast representing the state of North Carolina, where previous literature has investigated the Gulf Stream as an alternative renewable energy source to power hydrokinetic devices (Faria et al., 2022; Li et al., 2017).

ADCP measurements of ocean current velocity were obtained with the ECU Coastal Studies Institute (Haines et al., 2022) in 10 min time

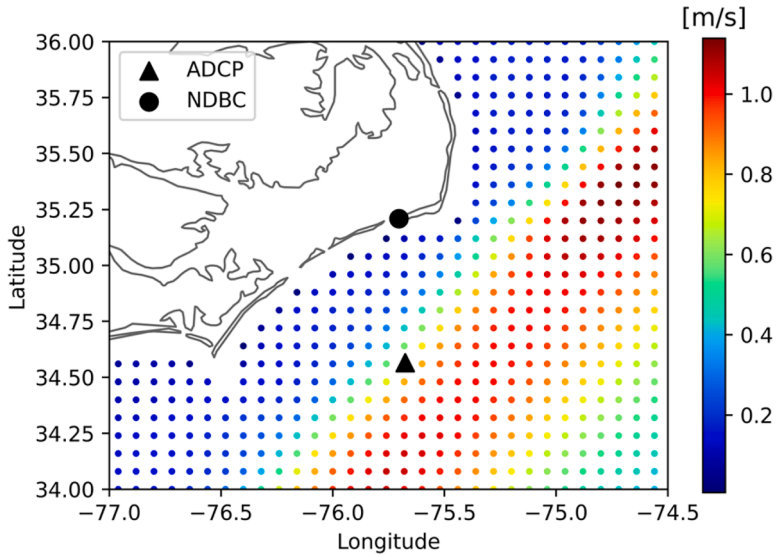

Fig. 4. ADCP and NDBC station together with the spatial distribution of the ocean current resource at 50 m Depth (HYCOM 1994–2021).

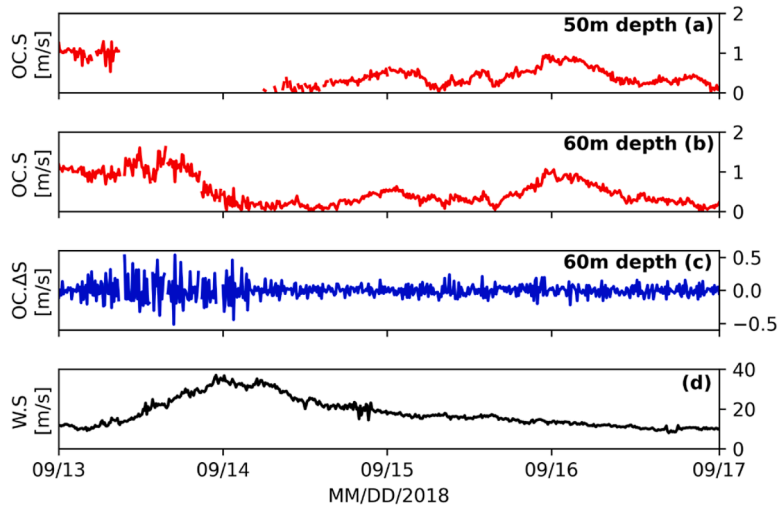

Fig. 5. Ocean and wind condition during hurricane Florence. (a) Ocean current speed at 50[m] (b) Ocean current speed at 60[m] depth; (c) Ocean current speed variation at 60[m] depth; (d) Wind speed.

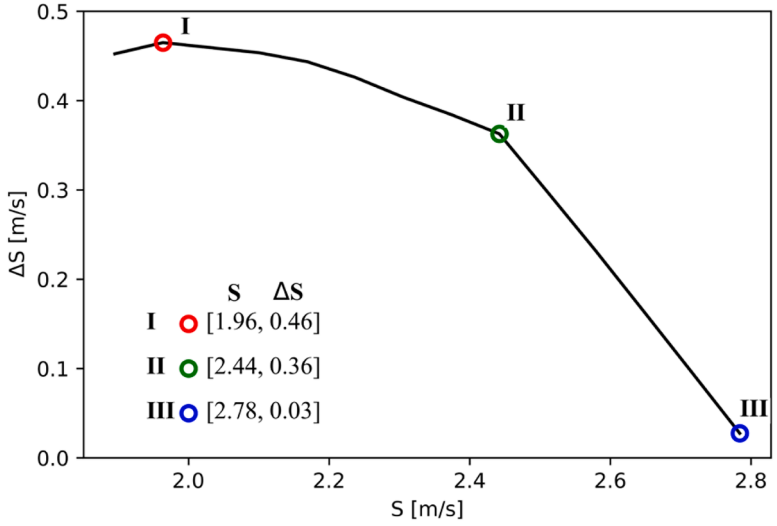

Fig. 6. 100-year recurrence curve: worst events every 100 years.

Table 1
Mean and quantiles (Confidence interval) for Model I and Model II (Conditioned on the normalized input data).

Parameter	Σ_{11}	Σ_{22}	ρ	$\beta_{0,s}$
Median	1.012	1.011	−0.267	0.001
2.5 % Quantile	0.820	0.816	−0.547	−0.155
97.5 % Quantile	1.271	1.270	−0.098	0.155
Parameter	$\beta_{1,s}$	$\beta_{0,\Delta s}$	$\beta_{1,\Delta s}$	λ
Median	−0.047	−0.001	−0.060	0.044
2.5 % Quantile	−0.200	−0.153	−0.208	0.029
97.5 % Quantile	0.105	0.155	0.094	0.064

discretization at 34.56° N latitude and 75.67° W longitude from April 2017 to November 2018, accounting for approximately 580 days worth of data or 84,000 10 min observations.

Although the ADCP measurements were available for horizontal and vertical current velocities, for simplicity, only horizontal velocities were used in this work, and in the definition of velocity variation during consecutive periods, changes in direction were not considered; ΔS_t is assumed to be the difference in velocity amplitude between betten $t+1$ and t ($\Delta S_t = S_{t+1} - S_t$). This work also assumes that the horizontal current direction is perpendicular to the ocean current device and mooring system, as shown in Fig. 3.

For wind speed, data were obtained from the National Data Buoy Center (NDBC) (NOAA, 2023) at 10 min resolution and 34.21° N longitude 75.70° W latitude, which corresponds to the NDBC anemometer closest to the ADCP covering the period of 2017 to 2018.

Fig. 4 shows the location of the ADCP device and NDBC station used in this study, together with the average Gulf Stream velocity estimates from 1994 to 2021 at 50 m depth using the HYCOM (2023) model. The Hybrid Coordinate Ocean Model (HYCOM) is an ocean circulation model developed as a multi-institutional effort sponsored by the National Oceanographic Partnership Program and has been used in many studies for the assessment of hydrokinetic resources (Halliwell, 2004; Kabir et al., 2015; Faria et al., 2023).

As previously mentioned in Section 2.4, the Reference Model 4 from SANDIA (Neary et al., 2014) is proposed for operation at 50[m] depth. Accordingly, all the statistical analyses described in Sections 2.2 and 2.3 considered only data from 40 to 60 m depth such that the relationship between the ocean variables $(S, \Delta S)$ and the depth (D) could be approximated as quasilinear.

Regarding the ADCP data, it is important to mention that turbulence

Table 2
Mean and quantiles (Confidence interval) for Model III (Conditioned on the normalized input data).

Parameter	Σ_{11}	Σ_{22}	ρ	$\beta_{0,s}$	$\beta_{1,s}$
Mean	1.009	0.820	-0.013	0.001	0.005
2.5% Quantile	0.832	0.676	-0.155	-0.140	-0.095
97.5% Quantile	1.245	1.011	0.126	0.140	0.192
Parameter	$\beta_{2,s}$	$\beta_{0,\Delta s}$	$\beta_{1,\Delta s}$	$\beta_{2,\Delta s}$	
Mean	0.006	-0.001	0.001	0.308	
2.5% Quantile	-0.085	-0.129	-0.132	0.044	
97.5% Quantile	0.209	0.127	0.134	0.574	

Table 3
Mooring system parameters.

Parameters	Steel chain	Polyester fiber rope
Mass per unit length [kg /m]	750	54
Equivalent cross-section area [m^2]	0.0955	0.0388
Diameter [mm]	200	280
Stiffness, EA [MN]	3600	392
CBS [kN]	30,688	23,000
Section length [m]	200	410

close to the air-sea interface can influence the ADCP measurements, leading to the loss of the ADCP return signal. Therefore, evaluating data across a range of depths (e.g., 40 m to 60 m) while applying the statistical analyses can help to compensate for the eventual missing data, strengthening the statistical model.

Fig. 5 shows the ocean current speed at 50 m (Fig 5a) and 60 m (Fig 5b) depth, the ocean current speed variation at 60 m depth (Fig 5c), and the wind speed (Fig 5d) during Hurricane Florence, a category four hurricane that hit the NC coast in September of 2018 (Stewart and Berg, 2019). From this figure, it is observed that a significant segment of data is missing at 50 m depth; and that at 60 m, the same time segment contains few missing measurements, justifying the need for using multiple depth measurements in the statistical analysis. Also, from Fig. 5c and d, it is possible to notice that the increase in ocean current speed variation coincides with the increase in wind speed.

Finally, even though ocean current speed data can be obtained from models such as HYCOM and MABSAB (HYCOM, 2023; Gong et al., 2015) at high spatial resolution covering large geographic areas, data at sub-hourly time discretization capable of capturing the anomalies that may occur during extreme weather events is not easily available. As a result, this study relies solely on ADCP measurements. However, ADCP data is often constrained due to several factors: the high cost of equipment and deployment, the logistical challenges of maintaining instruments in remote and harsh ocean environments, and the relatively sparse distribution of long-term measurement stations. The authors acknowledge the importance of expanding the dataset, both in terms of time period and geographic coverage, to improve the accuracy and reliability of future analyses.

4. Results

4.1. Fragility curve estimate for ocean current devices

Fig. 6 shows the 100-year recurrence curve for the site location investigated. This curve is generated following the procedure detailed in Section 2.2, where Model I is implemented using JAGS (Just Another Gibbs Sampler) (Depaoli et al., 2016) in R Programming Language. A Markov Chain Monte Carlo (MCMC) model (Reich and Ghosh, 2019) is used to sample the probability distribution of Model I (Bayesian Inference), with 10^6 iterations, thinning of one, two chains, and a burn-in of 10^4, which ensured that only samples from the equilibrium distribution

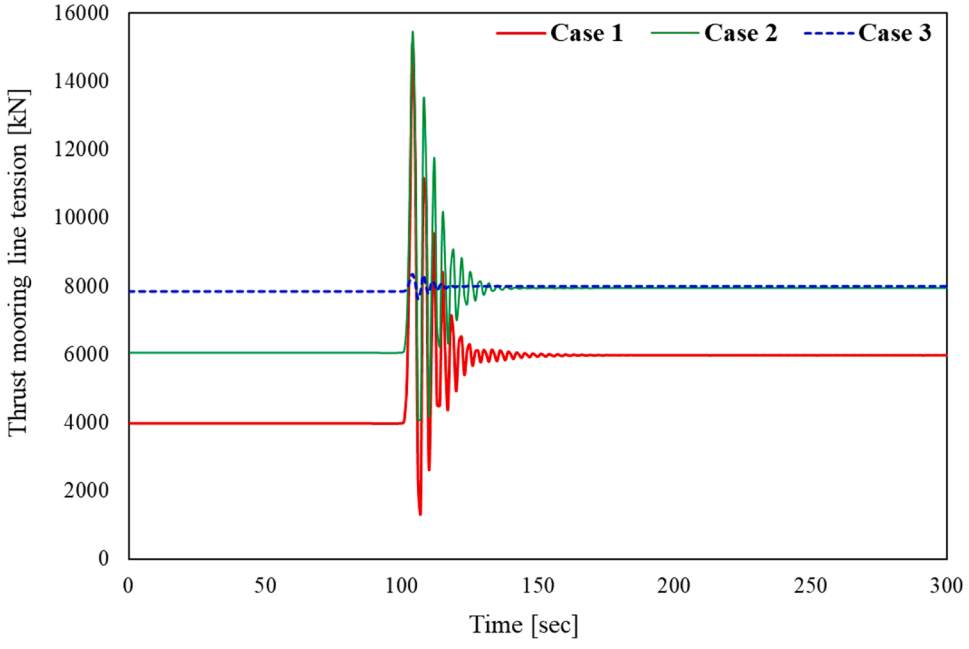

Fig. 7. Thrust mooring line tension versus time in different scenarios.

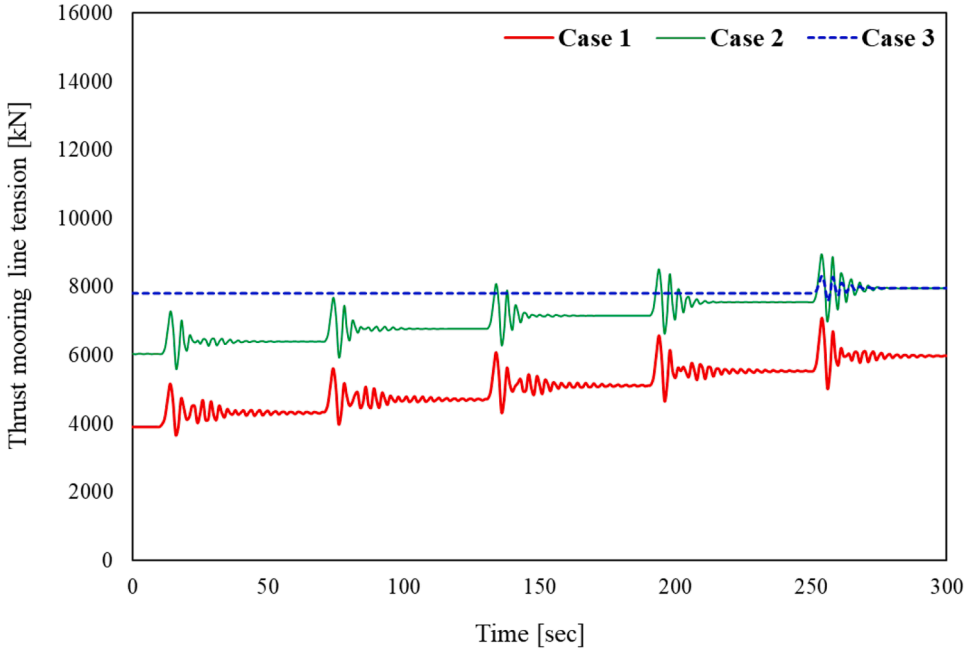

Fig. 8. Thrust Mooring line tension versus time in different scenarios.

were saved for later use. Furthermore, all model parameters converged with a Gelman-Rubin (Gelman and Rubin, 1992) statistic of 1.0. For more details regarding the confidence intervals of the parameters of each model, refer to Table 1.

From Fig. 6, we select three extreme ocean current conditions (I, II, and III) expected to repeat every 100 years and use these events in the mooring system modeling (Section 2.4).

4.2. Model III: probability distribution of current velocity and velocity variation under extreme winds

Similar to Model I, Model III was simulated in JAGS (Depaoli et al., 2016), with 10^6 iterations, thinning of one, two chains, and a burn-in of 10^4, converging with a Gelman-Rubin (Gelman and Rubin, 1992) statistic of 1.0 for all parameters.

Table 2 shows the confidence intervals for all parameters of Model III. From these results, we can notice a strong relationship between the wind speed condition and the ocean current velocity variation ($\beta_{2,\Delta s}$). It is important to mention that other works have documented similar behaviors during hurricane events (Todd et al., 2017; Ezer, 2018; Oey et al., 2006).

Regarding the other parameters of Table 2, no particular relationship can be immediately drawn. However, as the Bayesian modeling provides a probabilistic representation of each parameter of Model III, it also statistically limits the range of values that the parameters can assume, improving the representation of the probability density function of $(S, \Delta S)$ during extreme wind events.

4.3. Mechanical moorings model simulations

This section determines the minimum mooring line diameter that can withstand extreme ocean conditions over a 100-year period, following DNV code recommendations (DNV, 2015). Many combinations of line type, line size, location, and size of clump weights can be used to achieve a given target limit state. To minimize the number of variables in the analyses, the mooring scope, clump weight, buoyancy mooring line

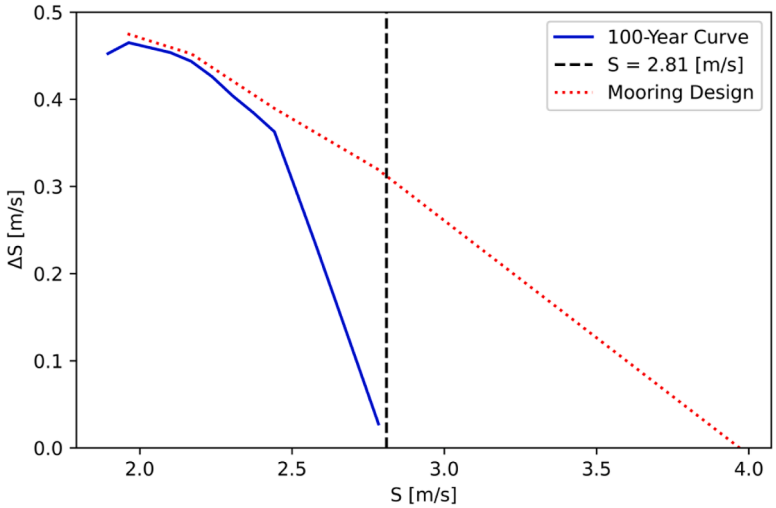

Fig. 9. (S, ΔS) operational limits of the system.

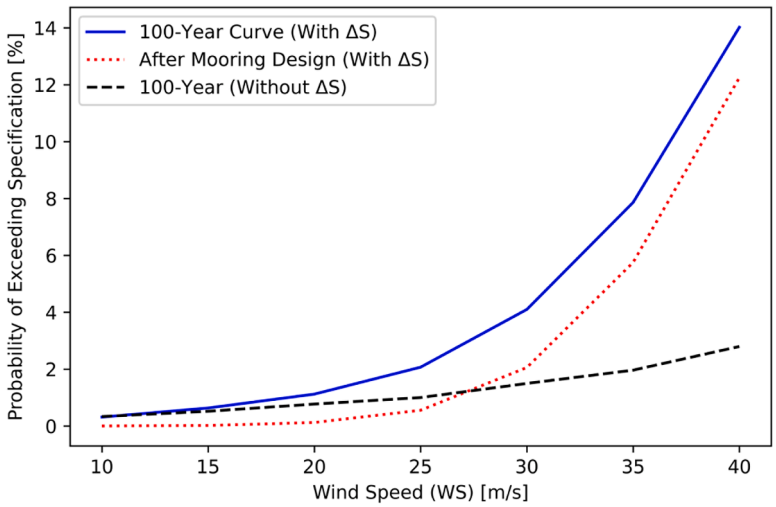

Fig. 10. Fragility curve of the ocean current device mooring system, considering different maximum operating limits.

properties, and steel chain section of the thrust mooring line are kept constant (Table 3). By adopting the same mooring line length in each system, the magnitude of the pre-tension would change. Pre-tension is defined as the component's tension when no environmental loads are acting on the unit or the mooring lines (Sauder and Tahchiev, 2020). Mooring line pre-tensions of about 10 % and 20 % of CBS are considered for steel chain and polyester mooring lines, respectively.

A worst-case scenario, leading to the highest mooring line tension, is considered to arise from a combination of the current velocity and the current velocity increment. Three different cases are considered, as shown in Fig. 6. The time domain responses of the thrust mooring line with a length of 610 m (including 200 m of steel chain with $D = 200$ mm and 410 m of polyester rope with $D = 280$ mm) are shown in Fig. 7 for the three cases studied. The device is in equilibrium with the initial current velocity for the first 2 min, and then, the current velocity is increased instantaneously. Initially, the device experiences higher motions with inertia, leading to dynamic amplification and higher tension in the thrust mooring line. Then, the tension in the mooring line reaches an equilibrium state. The final current velocities in cases 2 and 3 are almost the same, so the equilibrium tension is the same in both cases, as shown in Fig. 7. However, the dynamic tension is 80 % higher in case 2 than in case 3. In other words, as the current velocity increment increases, higher dynamic tension in the thrust mooring line is obtained. Moreover, the maximum tension in case 1 is approximately 3 % lower than in case 2; accordingly, a current velocity of 1.96 m/s with an increment of 0.46 m/s (case 1) would cause a higher dynamic tension compared to a current velocity of 2.44 with an increment of 0.36 m/s (case 2).

An important aspect while considering variations in the current velocity and their influence on the mooring system response is the time interval at which these speed changes occur. Since the ADCP measurements are taken every 10 min, it is not clear how long it takes in each case to ramp to the final velocity. To investigate this condition, the current speed is increased through 5 steps in a total of 4 min. As can be seen in Fig. 8, the final maximum mooring line tension in all three cases is lower than the values shown in Fig. 7, where the current speed increment is applied instantaneously. However, in the absence of knowing the ramping time, the use of an instantaneous velocity increment is more conservative as it leads to the highest expected dynamic effect.

Finally, for the modeling approaches presented in Figs. 7 and 8, and considering the three different cases explored in each figure, case 2, with a final current velocity of 2.78 m/s, is the worst case. Also, by applying partial safety factors to the dynamic and mean components of the mooring line tension in case 2 (Eq. (19)), it is concluded that the mooring line with the adopted parameters can withstand the 100-year extreme ocean current conditions. Lastly, Fig. 9 shows the 100-year recurrence curve, and the (S, ΔS) operational limits of the mooring line design described in Table 3, while adopting the modeling considerations of Fig. 7.

4.4. Fragility curve estimate

As discussed in Section 2.5, fragility curves represent the probability of a system exceeding its maximum operational limits. For the mooring system examined in this study, Fig. 9 highlights several potential theoretical limits worth investigating.

Assuming no dynamic tension component, the maximum operating limit of 2.81 m/s (black line in Fig. 9) corresponds to the 100-year extreme current velocity. Conversely, if dynamic tension (including ocean current speed and variations) is considered, the 100-year recurrence curve can be approximated by the blue lines in Fig. 9. These two curves do not account for safety factors and are based solely on ocean current statistics without incorporating mooring system simulations. Section 2.4 discusses a standard for mooring system design (DNV, 2015), emphasizing the need for incorporating safety factors and conducting mechanical model simulations. Drawing on these standards, Section 4.3 defines a mooring design for the RM4 ocean current turbine, with its operational limits presented in red in Fig. 9.

In addition to determining the operational limits, this study also establishes the probability distribution of ocean current variables under extreme wind speed conditions (Section 4.2). Utilizing these operational limits and ocean current statistics, the probability of the equipment operating outside its specified range at a given wind speed can be computed as described in Section 2.5, thereby allowing for the determination of the mooring system fragility curves.

Fig. 10 shows the fragility curves estimated under different limits of operation. The solid blue line shows the fragility curve of the mooring system while considering the 100-year recurrence curve (Fig. 6) as the limit of operation, and the red dotted curve shows the fragility curve estimated after the mooring design specification, which creates extra capacity in the system as seen in Fig. 9. In both these cases, the dynamic component of the mooring system is considered not negligible, as in Section 4.3. Lastly, the black dashed line shows the fragility curve of the system if the dynamic component of the mooring line can be neglected. In this case, the maximum current speed expected to repeat every 100-year is 2.81 m/s, which is assumed as the limit of operation of the system. Since only wind speed measurements up to 40 m/s (90mph) are available in the dataset investigated, the fragility curve definition is limited based on this speed.

From Fig. 10, it is observed that if the transient effect of the speed variation is neglected (black line), the probability of exceeding the system specification at high wind speeds (*WS*) is 2 to 3 % at 40 m/s, and that it increases slowly with *WS* since the correlation between *WS* and ocean current speed (*S*) is not as evident as the correlation between *WS* and current speed variation (ΔS).

For the simulations that considered the transient effect related to the speed variation, the probability of exceeding the maximum system specification increases faster with *WS* as the strong positive correlation between ΔS and *WS* ($\beta_{2,\Delta s}$ in Table 2) increases the probability of events with larger ΔS values.

Finally, although the mooring system specification performed in Section 4.3 results in a design capable of enduring significantly more severe events than those estimated for the 100-year curve under low ΔS values (see Fig. 9 for S>2.78 m/s), few samples exist in this interval, as indirectly evidentiated by the black dashed line results in Fig. 10. This led to a small difference between using the 100-year curve and the limits of operation computed by the mechanical model simulation.

5. Conclusion

As offshore energy deployments increase in frequency and scale, understanding associated risks becomes crucial. While fragility curves exist for renewables like solar and wind energy, marine hydrokinetic devices lack such analyses, limiting our insight into their vulnerability. To address this gap, this study introduced a Bayesian modeling framework and mechanical model simulation to construct fragility curves, specifically for the mooring systems of marine hydrokinetic devices, associating the probability of equipment damage to extreme wind speed conditions (e.g., hurricanes).

The methodology proposed here is tested using acoustic current profile measurements from a site located off the North Carolina coast, and the RM4 ocean current device from Sandia. For this specific site, the Bayesian statistical analysis indicated a significant correlation between extreme wind speeds (e.g., due to hurricanes) and increases in current speed variation. Finally, mechanical model simulations were performed to determine the impact of this dynamic effect on the mooring line operation, and fragility curves that associate different wind speed conditions with the probability of equipment damage were constructed considering different modeling assumptions.

Our results demonstrate a strong statistical relationship between ocean current velocity variation and wind speed, highlighting the increased risk posed by hurricane events to ocean current turbine mooring systems. For instance, at 40 m/s wind speeds, there's a 12–14 % probability of equipment surpassing design specifications when considering dynamic ocean current variation, compared to 2-3 % if the dynamic effect is ignored.

The lack of well-established standards for designing and analyzing ocean current devices due to their early developmental stage underscores the significance of this research, as it lays the groundwork for consolidating knowledge and potentially establishing formal mooring system standards for these devices in the future. As such, future works should expand the analysis presented here, investigating the influence of extreme weather events on other components of marine energy devices. Particularly, for the mooring system of hydrokinetic devices, the methodology presented here should be explored while considering other site locations in an attempt to create a generalized fragility curve (not site-specific). Moreover, further investigation into the dynamic effects induced on mooring lines by ocean velocity variations is crucial. This study provided initial bounds of its impact, but a more comprehensive analysis accounting for the effects of direction changes on current velocity remains an important avenue for future research.

CRediT authorship contribution statement

Victor Augusto Durães de Faria: Writing – review & editing, Writing – original draft, Software, Methodology, Data curation. **Neda Jamaleddin:** Writing – review & editing, Writing – original draft, Software, Methodology, Investigation, Data curation. **Anderson Rodrigo de Queiroz:** Writing – review & editing, Supervision, Methodology, Funding acquisition, Conceptualization. **Mohammed Gabr:** Writing – review & editing, Supervision, Methodology, Conceptualization.

Declaration of competing interest

The authors declare that they have no known competing financial interests or personal relationships that could have appeared to influence the work reported in this paper.

References

Alves, J.H., Young, I.R., 2003. On estimating extreme wave heights using combined Geosat, Topex/Poseidon and ERS-1 altimeter data. Appl. Ocean Res. 25, 167–186. https://doi.org/10.1016/j.apor.2004.01.002.

ANSYS, 2013. ANSYS Fluent Theory Guide (Release 15.0). ANSYS Inc.

Bennett, J.A., Trevisan, C.N., DeCarolis, J.F., Ortiz-García, C., Pérez-Lugo, M., Etienne, B. T., Clarens, A.F., 2021. Extending energy system modelling to include extreme weather risks and application to hurricane events in Puerto Rico. Nat. Energy 6, 240–249. https://doi.org/10.1038/s41560-020-00758-6.

Caires, S., Sterl, A., 2004. 100-Year return value estimates for ocean wind speed and significant wave height from the ERA-40 Data. J. Clim. 18, 1032–1048. https://doi.org/10.1175/JCLI-3312.1.

Ceferino, L., Lin, N., Xi, D., 2023. Bayesian updating of solar panel fragility curves and implications of higher panel strength for solar generation resilience, 229. 10.1016/j.ress.2022.108896.

Chang, Y.C., Chu, P.C., Tseng, R.S., 2015. Site selection of ocean current power generation from drifter. Renew. Energy 80, 737–745. https://doi.org/10.1016/j.renene.2015.03.003.

Depaoli, S., Clifton, J.P., Cobb, P.R., 2016. Just Another Gibbs Sampler (JAGS): Flexible Software for MCMC Implementation, 41. American Educational Research Association and American Statistical Association, pp. 628–649.

DNV, 2010. Recommended practice DNV-RP-F205: global performance analysis of deepwater floating structures. Det Norske Veritas.

DNV, 2015. Offshore standard DNVGL-OS-E301: position mooring. Det Norske Veritas.

European Commission, 2020a. An EU strategy to harness the potential of offshore renewable energy for a climate neutral future. European Commission. Retrieved September 20, 2024, https://eur-lex.europa.eu/legal-content/EN/TXT/HTML/?uri=CELEX%3A52020DC0741.

European Commission, 2020b. Low Carbon Energy Observatory - Ocean Energy Technology Development Report. European Commission. https://dx.doi.org/10.2760/81693.

Ezer, T., 2018. On the interaction between a hurricane, the Gulf Stream and coastal sea level. Ocean Dyn. 68, 1256–1272. https://doi.org/10.1007/s10236-018-1193-1.

Faria, V.A., Queiroz, A.R., DeCarolis, J., 2022. Optimizing offshore renewable portfolios under resource variability. Appl. Energy 326. https://doi.org/10.1016/j.apenergy.2022.120012.

Faria, V.A., Queiroz, A.R., DeCarolis, J., 2023. Scenario generation and risk-averse stochastic portfolio optimization applied to offshore renewable energy technologies. Energy 270. https://doi.org/10.1016/j.energy.2023.126946.

Faria, V.A., 2024. Predictive and prescriptive analytics applied to energy systems. Ph.D. dissertation, North Carolina State University. Retrieved September 2024, from https://www.lib.ncsu.edu/resolver/1840.20/41952.

Gelman, A., Rubin, D.B., 1992. Inference from iterative simulation using multiple sequences. Stat. Sci. 7, 457–511. https://doi.org/10.1214/ss/1177011136.

Goodman, J.N., 2015. Performance Measures for Residential PV Structural Response to Wind Effects. Georgia Institute of Technology.

Gong, Y., He, R., Gawarkiewicz, G.G., Savidge, D.K., 2015. Numerical investigation of coastal circulation dynamics near Cape Hatteras, North Carolina, in January 2005. Ocean Dyn. 65, 1–15. https://doi.org/10.1007/s10236-014-0778-6.

Haas, K.A., Fritz, H.M., French, S.P., Neary, V.S., 2013. Assessment of Energy Production Potential from Ocean Currents Along the United States Coastline. Georgia Tech Research Corporation.

Haines, S., Muglia, M., Bahr, F., Hogue, B., Taylor, P., DeSimone, N., Matthias, G., 2022. Mooring data report for the processes driving exchange at cape Hatteras (PEACH) program. Retrieved August 2022, from https://zenodo.org/record/6380852#.Yw9vxXbMJQI.

Halliwell, G.R., 2004. Evaluation of vertical coordinate and vertical mixing algorithms in the Hybrid-Coordinate Ocean Model (HYCOM). Ocean Model. 7, 3–4. https://doi.org/10.1016/j.ocemod.2003.10.002 (Oxf).

Huang, A., Wand, M.P., 2013. Simple marginally noninformative prior distributions for covariance matrices. Bayesian Anal. 8. https://doi.org/10.1214/13-BA815.

HYCOM, 2023. GOFS 3.1: 41-layer HYCOM + NCODA Global 1/12° reanalysis. Retrieved September 20, 2024, from https://www.hycom.org/dataserver/gofs-3pt1/reanalysis.
IEA - International Energy Agency, 2021. Net Zero by 2050 A Roadmap For the Global Energy Sector. IEA.
IEC, 2015. IEC TS 62600-10: Marine Energy - Wave, Tidal and Other Water Current Converters - Part 10: Assessment of Mooring System For Marine Energy Converters (MECs). International Electrotechnical Commission.
Kabir, A., Lemongo-Tchamba, I., Fernandez, A., 2015. An assessment of available ocean current hydrokinetic energy near the North Carolina shore. Renew. Energy 80, 301–307. https://doi.org/10.1016/j.renene.2015.02.011.
Kakareko, G., Jung, S., Mishra, S., Vanli, O.A., 2021. Bayesian capacity model for hurricane vulnerability estimation. Struct. Infrastruct. Eng. 17, 638–648. https://doi.org/10.1080/15732479.2020.1760318. Maintenance, Management, Life-Cycle Design and Performance.
Kuang, J., Chen, G., Yuan, Z., Qi, X., Yu, Q., Liu, Z., 2022. Dynamic interactions of a cable-laying vessel with a submarine cable during its landing process. JMSE 10, 774. https://doi.org/10.3390/jmse10060774.
Li, B., Queiroz, A.R., DeCarolis, J.F., Bane, J., He, R., Keeler, A.G., Neary, V.S., 2017. The economics of electricity generation from Gulf Stream currents. Energy 134, 649–658. https://doi.org/10.1016/j.energy.2017.06.048.
Liu, T., Wang, B., Hirose, N., Yamashiro, T., Yamada, H., 2018. High-resolution modeling of the Kuroshio current power south of Japan. J. Ocean Eng. Mar. Energy 4, 37–55. https://doi.org/10.1007/s40722-017-0103-9.
Neary, V.S., Previsic, M., Jepsen, R.A., Lawson, M.J., Yu, Y.H., Copping, A.E., Fontaine, A.A., Hallett, K.C., Murray, D.K., 2014. Methodology for Design and Economic Analysis of Marine Energy Conversion (MEC) Technologies. Sandia National Laboratories.
NOAA, 2023. National Data Buoy Center. Retrieved September 20, 2024, from https://www.ndbc.noaa.gov/.
Oey, L.Y., Ezer, T., Wang, D.P., Fan, S.J., Yin, X.Q., 2006. Loop current warming by Hurricane Wilma. Geophys. Res. Lett. 33. https://doi.org/10.1029/2006GL025873.
Rahayuningsih, S., Djatmiko, E.B., Handayanu, H., 2020. Dynamic mooring lines tension of FPU operated at Madura Strait. IOP Conf. Ser. Earth Environ. Sci. 557. https://doi.org/10.1088/1755-1315/557/1/012071.
Reich, B.J., Ghosh, S.K., 2019. Bayesian Statistical Methods. CRC Press.
Rose, S., Jaramillo, P., Small, M.J., Apt, J., 2013. Quantifying the hurricane catastrophe risk to offshore wind power. Risk Anal. 33, 2126–2141. https://doi.org/10.1111/risa.12085.
Sauder, T., Tahchiev, G.. From soft mooring system to active positioning in laboratory experiments. https://doi.org/10.1115/OMAE2020-19103.
Stewart, S.R., Berg, R., 2019. National Hurricane Center Tropical Cyclone Report. NOAA, Hurricane Florence.
Todd, R.E., Asher, T.G., Heiderich, J., Bane, J.M., Luettich, R.A., 2017. Transient response of the gulf stream to multiple hurricanes in 2017. Geophys. Res. Lett. https://doi.org/10.1029/2018GL079180.
VanZwieten, J.H., Seibert, M.G., Ellenrieder, K., 2014. Anchor selection study for ocean current turbines. J. Mar. Eng. Technol. 13, 59–73.
Watson, E.B., Etemadim, A.H., 2020. Modeling electrical grid resilience under hurricane wind conditions with increased solar and wind power generation. IEEE Trans. Power Syst. 35, 929–937. https://doi.org/10.1109/TPWRS.2019.2942279.
White House, 2021. FACT SHEET: Biden administration jumpstarts offshore wind energy projects to create jobs. Retrieved September 20, 2024, from https://www.whitehouse.gov/.
Xu, K., Larsen, K., Shao, Y., Zhang, M., Gao, Z., Moan, T., 2021. Design and comparative analysis of alternative mooring systems for floating wind turbines in shallow water with emphasis on ultimate limit state design. Ocean Eng. 219. https://doi.org/10.1016/j.oceaneng.2020.108377.
Young, I.R., Kirezci, E., Ribal, A., 2020. The global wind resource observed by scatterometer. Remote Sens. 12. https://doi.org/10.3390/rs12182920.